NASA Technical Memorandum 104351

Model Rotor Icing Tests in the NASA Lewis Icing Research Tunnel

Robert J. Flemming
United Technologies Corporation
Stratford, Connecticut

Randall K. Britton
Sverdrup Technology, Inc.
Lewis Research Center Group
Brook Park, Ohio

and

Thomas H. Bond
National Aeronautics and Space Administration
Lewis Research Center
Cleveland, Ohio

Prepared for the
68th Meeting of the Fluid Dynamic Panel Specialists Meeting on Effects of Adverse Weather on Aerodynamics
sponsored by the Advisory Group for Aerospace Research and Development
Toulouse, France, April 29 - May 1, 1991

MODEL ROTOR ICING TESTS IN THE NASA LEWIS ICING RESEARCH TUNNEL

Robert J. Flemming
Senior Design Engineer
Sikorsky Aircraft Division, UTC
6900 Main Street
Stratford, Connecticut 06601-1381
USA

Randall K. Britton
Icing Research Engineer
Sverdrup Technology, Inc.
NASA Lewis Research Center Group
2001 Aerospace Parkway
Brookpark, Ohio 44142
USA

and

Thomas H. Bond
Aerospace Engineer
NASA Lewis Research Center
21000 Brookpark Road
Cleveland, Ohio 44135
USA

SUMMARY

Tests of a lightly instrumented two-bladed teetering rotor and a heavily instrumented sub-scale articulated main rotor were conducted in the NASA Lewis Research Center Icing Research Tunnel (IRT) in August 1988 and in September and November 1989, respectively. The first was an OH-58 tail rotor which had a diameter of 1.575 m (5.17 ft) and a blade chord of 0.133 m (5.25 in.), and was mounted on a NASA designed test rig. The second, a four bladed articulated rotor, had a diameter of 1.83 m (6.00 ft) and the 0.124 m (4.9 in.) chord blades were specially fabricated for this experiment. This rotor was mounted on a Sikorsky Aircraft Powered Force Model, which enclosed a rotor balance and other measurement systems. The models were exposed to variations in temperature, liquid water content, and median droplet diameter, and were operated over ranges of advance ratio, shaft angle, tip Mach number (rotor speed), and weight coefficient to determine the effect of these parameters on ice accretion. In addition to strain gage and balance data, the test was documented with still, video, and high speed photography, ice profile tracings, and ice molds. This paper presents the sensitivity of the model rotors to the test parameters, and compares the results to theoretical predictions. Test data quality was excellent, and prediction methods for ice accretion and rotor performance reproduced the respective trends observed in the test. Adjustments to the correlation coefficients to improve the level of correlation in the performance predictions are suggested in this paper.

LIST OF SYMBOLS

CL/σ lift coefficient/solidity

CQ/σ torque coefficient/solidity

LWC liquid water content, g/m^3

MVD droplet diameter, um

T static air temperature, °C

σ solidity

μ advance ratio

ΩR rotor tip speed

Δ change over a period of time due to icing

INTRODUCTION

Because of the trend toward design of all-weather rotorcraft, it is necessary to develop and validate experimental techniques to understand the effects of ice on rotor performance and to determine the design requirements for rotor ice protection. Analytical methods are now being developed to predict rotor performance in icing, including ice accretion and ice shedding. The use of a model rotor to provide a less expensive and more repeatable source of test data will aid in the validation of these analytical methods and support the overall goal toward more expedient certification procedures. The French undertook a model icing program where a 1/4-scale model rotor was tested in the ONERA S1MA wind tunnel at Modane, France (Ref. 1). This testing showed that a model program had promise, but the data acquired were too limited to provide a correlation base. However, this testing prompted the interest of rotorcraft icing researchers in the United States. NASA Lewis Research Center undertook a program with a university and industry consortium to demonstrate the usefulness of the model rotor test technique as an approach for obtaining meaningful icing data for rotating systems (Ref. 2).

TECHNICAL APPROACH

The Rotor Icing Consortium operated under a NASA Lewis Research Center (Lewis) grant to Texas A&M University, which then subcontracted work to each of the four major U.S. helicopter companies: Bell Helicopter Textron, Boeing Helicopters, McDonnell Douglas Helicopters, and Sikorsky Aircraft Division of United Technologies. The consortium worked during the early part of the program to identify the necessary tasks and the means to achieve them, and each of the members had specific responsibilities that lead to the successful testing of the two models. The U.S. Army Aviation Research and Technology Activity-AVSCOM provided additional funding (Propulsion Directorate), and icing tunnel hardware support (Aeroflightdynamics and Propulsion Directorates) during the actual testing.

A two model approach was selected as the most effective means to accomplish the program goals. A lightly instrumented OH-58 tail rotor (Fig. 1) that had been modified to approximately operate as a main rotor was chosen as the initial test article. This would be followed by the more sophisticated Sikorsky Powered Force Model (PFM) (Fig. 2) to provide detailed rotor performance measurements. The OH-58 IRT entry established operational techniques for the more complex model and gathered preliminary data. Ice was accreted on the blades in a variety of rotor and tunnel operating conditions and documentation of the resulting shapes was performed. The OH-58 model test was completed in October 1988 (Ref. 3).

The initial PFM IRT entry was scheduled for an 8 week period during July to September, 1989. During this time the model was installed and icing testing began. A total of 44 icing

encounters occurred in the 14 days of testing. At the end of this initial test period, the model was removed and a second entry scheduled for November 1989. Between tests, the model was serviced, data reviewed, high speed motion picture capability added, and methods for improving blade track were prepared. This second entry resulted in 41 icing encounters in 8 test days, expanded the temperature envelope, and included variations in liquid water content and droplet diameter (Refs. 4 to 6).

MODEL AND FACILITY DESCRIPTIONS

Icing Research Tunnel

The IRT (Fig. 3) is a closed-loop refrigerated wind tunnel. A 5000 hp fan provides airspeeds up to 134 m/sec (300 mph). The 21 000 ton capacity refrigeration heat exchanger can vary the total temperature from -1.1 to -42 °C. The spray nozzles provide droplet sizes from approximately 10 to 40 μm median volume diameter (MVD) with liquid water content (LWC) ranging from 0.2 to 3.0 g/m^3. The tunnel test section is 1.8 m (6 ft) high and 2.7 m (9 ft) wide.

Armor plates were attached to the walls of the tunnel test section during the model rotor test to protect personnel in the control room. Video systems were installed to monitor the test area and ice accretions on the blades, and to provide tracking information. For several runs 0.635 mm (0.025 in.) aluminium sheets were placed on energy absorbing material and attached to the armor plating in line with the rotor disk plane. The shed ice made permanent dents in the sheets that will be calibrated to calculate the impact energy of the ice that struck them. A high speed 16 mm camera was used to capture ice shedding from the blades. The movies were taken at 2000 frames per second and capture approximately a 60° arc of the rotor rotational field. These results will not be discussed in this paper.

OH-58 Tail Rotor

The tail rotor assembly was composed of the tail shaft, hub, teetering components,and rotor blades from an OH-58 helicopter. The rotor blades had NACA 0012 airfoils with a chord of 0.133 m (5.25 in.) and a span of 0.73 m (28.74 in.). The total diameter of the rotor assembly is 1.575 m (5.17 ft) (Fig. 1). This assembly was mated, through an adapter, to a 2.1 m long NASA-designed drive shaft. The extended drive shaft allowed the rotor blades to be run in the horizontal plane in the middle of the test section of the IRT while the 40 hp motor and other drive system hardware remained below the tunnel turntable (Fig. 4). A hydraulically operated collective pitch control provided the ability to change blade angle quickly to the desired condition. The drive housing was bolted to the tunnel floor plate via two gimbal pins. For this test the rotor shaft was set at 5° forward tilt to simulate forward flight of a helicopter.

A differential measuring device recorded reaction torque changes from the drive system. A set of redundant rotational speed pick-ups were located on the drive shaft.

Vibration output was recorded to detail the severity and timing of shedding events with respect to the torque data. Motor horsepower was calculated and recorded to verify the torque data. Finally, the collective pitch angle was noted to document the rotor blade angles for the specific icing encounters.

Powered Force Model

The Sikorsky PFM is a self-contained, general purpose rotor test rig. The load measuring systems, rotor power, and control mechanisms are located within the model frame. The rig is capable of accepting a fuselage and powered tail rotor, each containing its own balance system. For this project, only the main rotor balance was installed. The main rotor was located 1.01 m (3.33 ft) above the tunnel floor, about 0.10 m (0.33 ft) above the tunnel centerline. The US Army UH-60A model skins were used to enclose the balance and rotor hardware (Fig. 2). While the fuselage skins are scaled for a 2.86 m (9.37 ft) rotor, tunnel dimensions dictated the use of a 1.83 m (6.00 ft) rotor for this test.

The rotor head used for this project (Fig. 5) was a Sikorsky-designed NASA Langley owned general purpose, four bladed, fully articulated head with coincident flap and lag hinges at the 8.3 percent (76 mm or 3.00 in.) radial station. The hub has adjustable lead-lag dampers and for this test it had a zero pitch-flap coupling (δ_3). In order to preserve a consistent lead-lag damping coefficient during the variation in IRT temperature, the rotor viscous dampers were electrically heated to maintain the fluid at about 10 °C. Potentiometers mounted on the flap, lead-lag, and pitch axes provide positional information for the rotor system relative to the shaft.

The PFM main rotor was driven by two Able 3-phase variable frequency induction electric motors. As installed, the motors can rotate at speeds up to 8000 rpm. A 3.5 to 1 reduction gear box operates the rotor shaft speed to a maximum of 2286 rpm, which equates to a rotor tip speed of 219 mps (718 fps). Each motor has a continuous rating of 60 hp. Rotor speed was measured using an optical encoder. Model power was supplied by a variable frequency motor-generator set provided by the Aeroflightdynamics Directorate, US Army Aviation Research and Technology Activity. The motor-generator set featured a digital closed-loop rpm feedback control, which maintained a set rotor speed under the power variations that occurred due to ice accretion, shedding and control changes.

The rotor forces and moments (except torque) were measured using a strain gage balance, gimbal-mounted to the model frame with a soft spring attachment. The balance was electrically heated to maintain it at the calibration temperature of 20 °C. Rotor torque was obtained by measuring the reaction force between the gearbox (which was mounted on bearings) and the gearbox frame with a load cell. A 102 channel slipring was used to transfer the rotating system signals from blade gages, pushrods, motion hardware, and accelerometers to the fixed system. It also provided power to the damper heaters. The swashplate control components consisted of rotating pushrods and scissors, the swashplate, three electromechanical actuators, and a stationary scissors. Control inputs were made at the control console with cyclic and collective joystick controllers. The input signals were electronically mixed by the controller which then moved the model actuators. Resolved shaft axis cyclic and flapping first harmonic coefficients were obtained from potentiometers located on the rotorhead. These values were displayed graphically and numerically to facilitate rotor trimming. Shaft angle for this test was set using a remotely driven linear actuator located on the test rig support frame. A pitch arm transferred the linear motion of the actuator to the rotating motion of the

model shaft. This resulted in both a translational and model pitch motion for the rotor. The model support shaft angle range was from -10 to +3°. The angles set by the shaft angle control were corrected by the gimbal deflection angle and aerodynamic wall corrections to obtain the true total shaft angle.

The main rotor blades were designed and built by the McDonnell Douglas Helicopter Company using molds built by Sikorsky Aircraft. The blades had NACA 0012 airfoils with a chord of 0.124 m (4.88 in.), a -10° linear twist, and a taper ratio of 1. In order to stay within rotorhead stress limits at the design speed, the blade weight was kept to a minimum. This resulted in a thin walled hollow spar, an unsupported trailing edge, and an unpainted airfoil surface. Two of the blades were instrumented with strain gages in the flatwise, edgewise, and torsional axes to provide blade loading information for safety of flight. The data from the edgewise strain gages proved to be very useful in identifying shedding events. This prompted the addition of root edge-wise strain gages to the noninstrumented blades prior to the second entry. The rotor blades were marked on their upper surfaces with the blade number and spanwise decade percentage marks to provide identification of the blade being monitored and the relative location of the ice that was shed (Fig. 2).

DATA SYSTEM AND INSTRUMENTATION

The test techniques used in the IRT were developed during the July to October 1988 OH-58 tail rotor entry in the tunnel and used during the PFM test. Each icing run was recorded on the Dynamic Data Acquisition System (DDAS) and video systems. The video provided a viewing history of the ice accretion and shedding. There were three separate video systems: one for safety monitoring, one for blade tracking (which also provided good ice profile shapes near the blade tip), and one that allowed close-up images of the rotor blades. The three systems were strobe driven by a signal off the rotor shaft angle encoder. This gave a "frozen" image of the blade. The close-up data video system was installed on a tilt and pan mechanism along with a 35 mm camera that had a 400 mm zoom lens. The data video system had the capability of traversing the entire diameter of the main rotor while allowing zoom shots of as small a span as 0.10 m (3.94 in.) of the blade leading edge. The 35 mm camera was focused on the same close-up viewing area as the video camera, allowing pictures with greater resolution and clarity to be taken. Both the data video and the 35 mm camera were triggered from the same strobe to provide an accurate replication of the video image for the 35 mm camera.

The measured PFM test parameters fell into two main categories - those that were of research interest and those that were required solely for safety-of-flight. The parameters in the first category were processed by the DDAS and saved on both digital tape and floppy disks. Derived parameters were also computed using the DDAS and saved for further analysis. The test parameters used for analysis are the following:

Main rotor balance loads
- Normal force element number 1
- Normal force element number 2
- Axial force element
- Side force element number 1
- Side force element number 2
- Rolling moment element

Main rotor torque load
Main rotor speed
Tunnel parameters
- Total temperature
- Static pressure

- Total pressure
- Johnson-Williams Liquid Water Content

Instrumented blade positions
- Collective pitch
- Lateral cyclic pitch
- Longitudinal cyclic pitch
- Lead-lag angle
- Pitch angle
- Flapping angle
- Resolved lateral flapping angle
- Resolved longitudinal flapping angle
- Resolved coning angle

Model strut angle

Pushrod loads
- Blade number 1
- Blade number 3

Accelerations
- Gimbal lateral
- Gimbal longitudinal
- Rotor head aligned to blades 1 and 3
- Rotor head aligned to blades 2 and 4

Blade loads
- Flatwise load at blade station 11.4
- Flatwise load at blade station 16.5
- Flatwise load at blade station 21.7
- Flatwise load at blade station 26.9
- Edgewise load at blade station 11.4
- Edgewise load at blade station 16.5
- Edgewise load at blade station 21.7
- Edgewise load at blade station 26.9
- Root torsional load at blade station 10.1
- Torsional load at blade station 11.6 (r/R = 0.32)
- Torsional load at blade station 27.3 (r/R = 0.28)
- Blade 1 root edgewise load at blade station 10.1
- Blade 2 root edgewise load at blade station 10.1
- Blade 3 root edgewise load at blade station 10.1
- Blade 4 root edgewise load at blade station 10.1

A number of the derived parameters from the transducer outputs were computed and displayed at a rate of once per second to allow the model operator and Safety Of Flight (SOF) engineer to monitor loads and set target test conditions. These values accounted for tunnel blockage and buoyancy corrections, coordinate transformations, moment transfers, and balance interactions.

The heart of the DDAS digital system was a Digital Equipment Corporation PDP11/34 minicomputer. Simultaneous sample and hold amplifiers froze the analog channels before digitizing to maintain time correlation of each parameter in each time frame (i.e., in each data snapshot). Data were acquired at a rate of 16 samples per rotor revolution during the icing test. Data acquisition hardware and software were developed to reduce the quantity of stored data. Data were digitized only for the first 10 revolutions of each second (160 samples per data burst), and transferred from the DDAS to a PC/AT computer for further processing.

An integral part of the DDAS processing was the correction of the wind tunnel data for the effects of the tunnel walls. These corrections increase the effective tunnel speed and alter the rotor wake flow angles. Use of nondimensional terms normalize the data for day-to-day changes in ambient pressure, rotor speed fluctuations, and temperature variations. Data corrections must also be made for shaft torque tares, gravity tares, the induced angle of attack, and three dimensional buoyancy and solid blockage effects. The coordinate systems, data correction equations, and a description

of the derived parameters will be included in a future NASA Contractor Report.

TEST PROCEDURE

During the test run, information was collected on the data systems and the video systems, and the tunnel conditions were monitored. Liquid water content information (rise time, cloud stabilization, and spray bar lag from spray initiation) was recorded from the Control Room console output. A Johnson-Williams (J-W) LWC meter was also used during the PFM test.

Post-run information was gathered by taking 35 mm camera photographs, recording ice tracings, noting visual observations, and making ice molds. Pictures were taken of the blade planform, an end profile, and any unusual ice formations. Close-up shots of ice growths were taken to record their minute detail. A heated aluminum block with a cut-out contour of the airfoil shape was used to make a clean slice through the ice formation. A template was then held against the ice shape and a tracing made. Measurements of the ice thickness along the profile were taken at various chord locations. Visual observations were recorded about the kind of ice, any secondary growth, and frost formation. Molds were taken for several test conditions during each test.

The liquid water content and droplet diameter of the spray cloud are dependent on the spray bar water and air pressures, and the tunnel velocity. The pressure values are generated from a set of calibration equations. The above approach gives an accurate setting for LWC, but it does not provide any history of the spray which is necessary to understand the cloud time lag between spray on and model inundation, rise time to the target LWC, and cloud characteristics during the spray. A Johnson-Williams (J-W) liquid water content meter was installed during the PFM test slightly in front of and below the rotor (Fig. 2), providing cloud time history information.

TEST DATA

Accuracy and Repeatability

The ability to repeat a test condition was a major goal of this test program. Rotorcraft icing flight test data has been subject to considerable data scatter, making the application of that data to code validation and basic research difficult. A portion of the observed scatter occurs due to variations in the accretion of ice on an airfoil (Ref. 7), but most of the scatter comes from uncontrolled variation in the cloud. The IRT provides a much more controlled environment as is shown by the LWC repeatability for two settings in Fig. 6. The trends from the IRT test data show some scatter, but the data appear to be of much better quality than previous data available in the public domain. Overall ice shape repeatability was found to be very good during both tests. For a given set of rotor conditions and at a given radial location tracings of the two-dimensional shape were made and compared to obtain a measure of this repeatability. These two-dimensional shapes were found to agree best at colder temperatures where the formation was of a rime nature and was fairly smooth and easily traceable. The ice tracings tended to vary more at warmer temperatures due not necessarily to actual variation in the shapes but to difficulties in obtaining accurate tracings of these relatively small but complex geometries. However, even with the tracing difficulties the repeatability will be shown to be quite good at these warmer temperatures.

Figure 7 illustrates the quality of ice shape repeatability for one particular condition which was run several times during the OH-58 tail rotor test. As may be seen the ice shape at the measurement location was of a glaze nature with a slight double horn shape and some degree of roughness and secondary ice formation behind the primary shape. In making the cut in the ice to get to a two-dimensional tracing, often much of the detail in the secondary formations was lost due to melting when the cut was made. Some of the roughness and finer details of the primary shape were also affected by partial melting during the cut. Even with some loss of detail though, it can be seen that the ice shapes tended to repeat quite well from run to run. Because more care was taken later in the test to preserve the roughness and secondary formation detail, the final two tracings better illustrate the actual ice shape which existed at this condition throughout the rest of the OH-58 test. This same degree of two-dimensional ice shape repeatability was seen at other test conditions as well. Figure 8 shows ice shape comparisons for two different PFM repeat conditions and illustrates the small amount of variance between typical runs. The occurrances of ice shedding were also repeatable (Refs. 3 and 5). Figure 9 is a plot of lift and torque coefficients as a function of icing time for the PFM. Results for the 5 test runs show excellent repeatability. Other repeat conditions also showed very good agreement.

The accuracy of the OH-58 tail rotor torque measurement was not determined during the test. The 2σ accuracy of the PFM rotor loads was estimated to be:

Balance full scale, percent		Typical measurement, percent
Lift	0.2	1.1
Drag	.2	10.5
Torque	.7	2.5

TEST CONDITIONS

The test matrices were set up to include a range of conditions for a number of rotorcraft performance parameters under varied IRT conditions. For the OH-58 tail rotor test the temperature range was -6.7 to -26.1 °C, the LWC range was 0.25 to 0.50 g/m^3, and the MVD range was 10 to 15 μm. Maximum rotor tip speed was 173 mps (568 fps). For the PFM test the temperature range was -1.7 to -30.5 °C, the LWC range was 0.35 to 1.24 g/m^3, and the MVD range was 13 to 23 μm. The predominant PFM condition was at -15 °C, 0.50 g/m^3 LWC, and 15 μm MVD at a rotor tip speed of 206 mps (675 fps). Icing encounter times were from 44 to 158 sec. PFM thrust, propulsive force, advance ratio, and model rpm were changed, within the above tunnel conditions, to provide a wide scope of performance mapping.

OH-58 TAIL ROTOR DATA ANALYSIS

Ice accretion on the OH-58 tail rotor produced a rotor torque rise which was linear with time for a fixed set of rotor and tunnel conditions. The speed with which torque rose with time was dependent upon the specific rotor and tunnel conditions chosen. Below roughly 7° collective, the rate of torque rise with time in icing appeared relatively constant and

independent of collective. At collectives greater than 7° in icing, torque rise was more rapid. Clean rotor torques at high collectives also showed a significant increase in slope over the base torque at lower collectives, and any ice accreted on the blades will then further the torque rise.

The torque rise rate was also found to be dependent on cloud conditions (lower liquid water content and lower drop size give slower torque rise) and temperature (there is some "worst" temperature at which ice is predominantly glaze and extends to the tip without shedding). Because several different parameters affect the accretion and shedding characteristics of a system, the conditions which produce the highest torque rise rate will vary from one configuration to another. The worst case will most likely occur at some intermediate temperature which is conducive to glaze ice formation in the tip region. For this test that temperature appeared to be in the neighborhood of -15 °C.

Figure 10 presents a typical torque history in a case where multiple sheds occurred. Here torque rose smoothly until shedding occurred, at which time the torque dropped somewhat. As ice continued accreting on the blade, the torque rose again until another shed took place. If the accretion had been allowed to continue long enough, an "equilibrium" time would be reached at which shedding and accretion would roughly balance each other out. Torque would then level off at some final equilibrium value.

As expected, ice accretion on the rotor blades tended to increase vibration (measured with accelerometers) due to added mass on the blades and distortion of the flow field around the blades' leading edges. Because the accretion was symmetric, vibration rise before shedding was gradual. Occasionally, depending primarily on collective and somewhat on temperature, vibration rose to high enough levels to necessitate stopping the spray before any shedding occurred. Otherwise, vibration would rise gradually until shedding took place. At this time the vibration would either decrease if the blades shed relatively symmetrically or increase if the shedding occurred on only one blade. The direction and magnitude of the vibration change at shedding was generally sufficient to indicate symmetric or asymmetric shedding to the operator without any visual indicator.

A wide range of tunnel total temperatures from -26.1 to -6.7 °C were run in this test which encompassed the rime, mixed, and glaze ice regimes. Temperature was found to have a significant effect on the rotor ice accretion and shedding characteristics. Tunnel total temperature combined with the rotational effect of kinetic heating on the local blade temperatures influenced both ice type and transition location from rime to glaze ice. In addition, the existence and size of secondary ice formations typically in the form of ice feathers were affected by the local temperature. Figure 11 illustrates the change in ice type at a given location and condition over a range of tunnel total temperatures. The shedding characteristics are strongly influenced by temperature because of the material properties of ice. Above 23 °F, both the tensile and shear strength of impact ice decrease as the temperature increases (Ref. 8). Thus, at warmer temperatures one would expect to see see more shedding at shorter icing times. Although no concentrated study has been performed to date on shedding aspects of this test, this particular dependence on temperature was observed during the experiment.

Variations in cloud liquid water content (LWC) and median volumetric droplet diameter (MVD) were found to produce a measurable change in the accretion characteristics of the rotor blade ice formations. The liquid water content and drop size were always varied in tandem in the OH-58 tail rotor test, precluding determination of the effect of each specific parameter alone on the resulting ice shape, but the test still yielded insight into the changes which cloud parameters had on the resulting rotor ice shapes. The LWC/MVD combinations run in this test were 10 μm and 0.25 g/m^3, 12 μm and 0.40 g/m^3, and 15 μm and 0.50 g/m^3. Each produced markedly different accretions for a given set of conditions as Fig. 12(a) shows. Increasing the LWC/MVD had the effect of further encouraging glaze ice formation at a given temperature and given radial location.

Cloud liquid water content and drop size were seen to have a significant effect on rotor torque and vibration by influencing the size and type of ice which formed on the rotor blades. Each of the three sets of cloud conditions produced markedly different ice shapes and therefore distinctly different torque levels for a given rotor operating condition and temperature. As Fig. 12(b) illustrates, going from the clean blades to a 2-min icing spray at a liquid water content of 0.25 g/m^3 and median droplet diameter of 10 μm, caused no measurable change in torque. Further raising the cloud density to 0.4 g/m^3 and the droplet diameter to 12 μm raised the torque values by about 16 N-m. An even more substantial torque rise was produced by going to a liquid water content of 0.5 g/m^3 and droplet diameter of 15 μm. Here the torque was found to rise by about 32 N-m at each collective.

Rotor rpm was found to have a substantial effect on the nature of the ice which formed on the blades under a given condition. Increasing rpm had the effect of increasing the local velocity at some radial station which then encouraged a more glaze-oriented formation than did the lower speeds. This in turn had the effect of shifting the rime-to-glaze ice transition zone further inboard on the blade as rpm was increased. Figure 13 illustrates this rpm effect for a given set of conditions.

PFM DATA ANALYSIS AND CORRELATION

Baseline Data

The analysis presented in this section concentrates on the effect of icing time on performance parameters, primarily rotor lift and rotor torque. The hovering performance of the rotor was determined during tests in the Sikorsky model rotor test facility. The measured hover performance is compared with the model rotor predictions of the CAMRAD/JA code (Ref. 10). These data show that the rotor performance matched theory, using a Δc_d of 0.0026 to adjust the full-scale (chord = 0.41 m or 16 in.) NACA 0012 airfoil data for the effect of Reynolds number on profile drag. This profile drag increment is consistent with that derived using Ref. 11 methodology.

Determining the Onset of Icing

One step in the analysis of the effect of icing on a rotor is the determination of the time that the spray cloud reached the model, the onset of icing time. An accurate determination of the onset of icing is important to provide a valid reference

point for data and theoretical comparisons. The data were reviewed to determine experimentally the time for this onset of icing. This onset time was based on the Johnson-Williams (J-W) LWC probe (when available) or the beginning of the change in rotor torque and lift. This approach minimized random variations in spray development time and improves the overall data quality for the analysis for parameter comparisons.

Liquid Water Content

For this test, the duration of the spray generally ranged from 44 to 158 sec, including the spray stabilization time. The rate of ice accretion is directly related to the chord size. The smaller the chord, the faster the non-dimensional ice growth. Because of this, sub-scale experiments must use shorter spray times to simulate full-scale icing encounters. A plot of the J-W LWC data for a number of runs (Fig. 14) indicates that there was some rise time prior to reaching the target value (with the rise time increasing at the higher LWC runs). However, the spray condition remained relatively close to the desired setting after the ramp up. The cloud reached the model about 10 sec after the "spray on" command was given.

Ice Shedding

The ice shedding process is a very important factor in a propeller or rotorcraft icing encounter; this phenomenon dominates the outcome of the entire icing event. Figure 15 shows a plot of the root strain gage output for each of the blades as a function of time. When a shed occurred there was a large fluctuation in the strain gage reading. There were two major shedding events for this run; one at approximately 25 sec and another at about 38 sec. For both events blade number 4 experienced a shed first, followed by sheds from the other blades. Rotor torque, also shown in Fig. 15, exhibited a small reduction during minor shedding, with more pronounced changes in torque at major shedding events. There were instances where ice was shed asymmetrically, but the model vibration load limits were not exceeded. Figure 16 shows an example of a section of a blade with ice shed. While this shows a relatively clean break in the ice, the majority of the time there is some residual ice left on the blade after a shed.

Lift and Torque Increments

The rotor balance was sized to accommodate the vibratory loads due to ice shedding, and was, therefore too large to measure precisely the low propulsive force (power required to maintain a forward velocity) levels at the primary test speed of 31.1 m/sec (80 kt). However, the data show that shaft angle, and hence propulsive force, are of secondary importance in the data trends (Ref. 5).

The Δ lift data from the first of the two entries shows a rapid lift loss at the beginning of the ice encounter, indicative of a significant roughness effect on the lift curve shape. Data from the second entry does not exhibit the large initial lift loss, more consistent with current theoretical predictions (see Correlation with Theory section of this paper). Other data obtained in this test program show that variation in C_L/σ has no effect on lift loss or torque rise due to icing, i.e., the percent loss in lift and the percent rise in torque are independent of initial rotor lift.

The model was tested over an advance ratio range consistent with the blade envelope. For the advance ratio

range tested there is no statistically significant effect on either Δ lift or Δ torque.

The data followed expected trends when the LWC was increased. The torque data increased and the lift at constant collective pitch decreased (Fig. 17).

The median volume droplet diameter was changed in a range from 13 to 23 μm at a constant LWC of 0.75 g/m^3. The results indicate that an increase in MVD has the expected effect of increasing the torque and decreasing lift (Fig. 18).

Temperature was varied from near-3.7 to -30.5 °C. Figure 19 shows a plot of the power increase for temperatures ranging from -3.7 to -15.2 °C. The torque increases as temperature decreases because, in this temperature range, the radial icing extent increases and the outer extent is composed of more glaze ice than rime. As more of the rotor blade is iced the performance penalties become more severe. Figure 20 shows another plot of torque rise for a much colder temperature range, -15.2 to -30.5 °C. Here, the torque rise trend reverses and actually decreases with temperature. As the temperature decreases the ice shape changes from glaze to rime, and the performance penalties are less. Figures 19 and 20 show plots of the lift loss for these ranges of temperature. The trend is consistent with that of the torque with the exception of the extremely cold temperature (-30.5 °C).

The effects of icing on rotor torque at different tip speeds is shown in Fig. 21. For the higher tip speeds a balance between shedding and accretion appears to have been reached such that the torque levels off after roughly 50 sec of icing time. However, the torque trace for the lowest tip speed indicates a much higher torque towards the end of the data run, since this lower tip speed has not induced shedding.

Comparison With Theory

Comparison with theoretical methods can involve accretion, shedding, and rotor performance. The correlation presented in this paper uses LEWICE for ice accretion, and computes performance using the Sikorsky Generalized Rotor Performance (GRP) forward flight performance code with the rotorcraft icing subroutine of Ref. 7. This sub-routine is based on an empirical correlation with experimental data.

The ability to adequately predict a given ice shape is critical to a rigorous methodology which predicts performance degradation during an icing encounter. The results presented here were obtained with the computer analysis LEWICE (Ref. 12), which was developed at NASA Lewis. LEWICE is a two-dimensional code which, given the geometric and atmospheric conditions, will predict the cross-sectional ice shape for a specified icing time. Several comparisons have been made between the predictions of LEWICE and these experimental data (Ref. 6). The local angle of attack was determined with the Boeing Helicopters B65 computer performance code. The Mach number and angle of attack were azimuthally averaged for input into LEWICE as shown to be appropriate by Korkan, Dadone, and Shaw (Ref. 13) and Flemming and Lednicer (Ref. 7). The guidelines for time step size and surface roughness were those described by Korkan and Britton (Ref. 14). Figure 22 shows two sample comparisons for a rime condition. The overall agreement is quite good with slight overprediction by LEWICE on the lower

(pressure) surface. Detailed comparisons have been made for both rime and glaze conditions and the results have been encouraging (Ref. 6).

The icing correlation can be broken into two time regimes. The first regime exists prior to ice shedding, thereby limiting the analysis solely to a study of ice accretion. The second regime exists after ice shedding begins, adding a somewhat random factor to the correlation.

The correlation centered on prediction of incremental rotor lift ($\Delta C_L/\sigma$) and incremental rotor torque ($\Delta C_Q/\sigma$) for input shaft angles and flapping angles. Collective pitch was held constant at the predicted clean rotor trim solution and the performance of the rotor system was allowed to degrade. The ramp in LWC that occurred during the start of the icing encounter (Fig. 14) has been ignored and a step change assumed. Emphasis has been placed on the evaluation of the effects of tip speed, rotor lift, LWC, droplet diameter, icing time, and temperature on rotor lift and torque. These variables encompass the major terms in the Ref. 7 icing relationships.

A key element in the prediction of iced rotor lift and torque changes is the prediction of radial ice extent. Figure 23 shows a comparison between the observed ice extents from the PFM test and the Ref. 7 prediction. Since some shedding of ice may have occurred prior to the post run ice extent observations, it would be expected that the data would fall on or below the Ref. 7 line. The points that fall above the line imply that the Ref. 7 ice extent boundary temperature could be increased for future correlation work.

Figures 24 and 25 present the predicted effect of temperature on changes of lift and torque. The Ref. 7 method underpredicts warm icing cases. The observed ice extent from the warm temperature icing ranged in span from 32 to 49 percent. The predicted ice extent is 48 percent, excellent agreement considering that some ice may have shed from the blade between the ice accretion and the post tunnel shutdown observations. Ice thicknesses for these cases were not quantified, but the run log noted that the ice thicknesses were small. The predicted ice thickness ranges from 0.25 mm (0.01 in.) to 2.29 mm (0.09 in.), consistent with the "small thickness" observations. The large increments in power at warm icing temperatures have been reported by pilots, but these occurrences are not well documented. Further research in this area is warranted.

Once the blade is fully iced, comparison using Ref. 7 relationships is much better. Figures 24 and 25 show that the agreement is very good at -10, -15, and -20 °C. However, the prediction is conservative at colder temperatures. An examination of the predicted drag coefficients shows that the Ref. 7 code can produce rime drag coefficients that are greater than comparable glaze drag coefficients for small icing times. A reduction in rime drag coefficients can improve correlation significantly. The code has been modified to use glaze ice drag coefficients when those coefficients are less than the predicted rime ice drag coefficients.

CONCLUSIONS

Scaling

It should be noted that these tests did not deal with scaling in a truly rigorous way. The rotor chord was kept as large as possible in order to reduce Reynolds number effects. This resulted in a high solidity because tunnel geometry constrained the

rotor diameter. To minimize scale effects, the model was operated at full-scale tip speeds and full-scale tunnel speeds. Tunnel temperatures and pressures represent full scale conditions. These give a model Reynolds number that is lower than the full-scale value by a factor of the full to model scale chord ratio. While liquid water content and droplet diameter are important, spray cloud limitations prevented strict scaling of these parameters. Scale relationships have been presented to account for these effects (Refs. 4, 5, and 9).

CONCLUDING REMARKS

The testing of the OH-58 Tail Rotor Rig represented a positive and crucial first step in model rotor icing tests. Data gathered in this test was repeatable in terms of the nature of the accretions and their effect on rotor performance. Techniques for testing of a model rotor in an icing wind tunnel were developed and served to enhance the follow-on testing of the PFM, and set the capability for future testing of other models of rotating systems in icing.

The examination of the data from the Powered Force Model testing has provided encouraging results. The quality of the test data appears to be excellent. The changes in lift and torque are well documented and are remarkably repeatable. The model instrumentation clearly shows the time of shedding events.

The data show the effects of temperature, rotor speed, liquid water content, and droplet diameter on icing. The data trends are generally as expected. Test procedures established for rotorcraft testing in the IRT provided a safe operating environment and produced high quality data for performance analysis. The lift at a constant control collective dropped by up to 15 percent due to icing. Torque increases of 50 percent and more were common. The techniques employed have been validated by the results obtained, and the data will be useful for code and scaling research and development.

Comparisons were made between the experimental ice accretion data and the analysis of LEWICE. The results for the rime condition were excellent. Results for the glaze condition were mixed with a slight tendency to overpredict the thickness. Overall, it is felt that the predictability of the ice shape data was good.

Comparison of test results were made with the Sikorsky Generalized Rotor Performance (GRP) code predictions. Excellent prediction of moderate temperature ($-20^{\circ} < T < -10\ ^{\circ}C$) performance degradation was achieved. The code slightly overpredicted colder temperature torque rise due to an overprediction of rime ice profile drag. The code underpredicts warmer torque rise, a phenomenon that must be researched further.

Future Plans

The near term goal is the completion of the data analysis for the PFM entries and the continuation of correlation studies. High speed 16 mm movies will be processed, and this information used with the energy impact data to support ice accretion and shedding model development. Molds taken during the testing will be used to make ice castings for use in simulated ice experiments. The next experimental effort will be a re-entry of the OH-58 model rotor in the IRT with a calibrated impact energy measurement device. This test will concentrate on documentation and analysis of the ice shedding process.

Longer term goals include further PFM model icing tests, coordinated with full-scale rotorcraft icing flight testing. This would follow a logical progression for development and verification of the model rotor test techniques and the analytical methods, and identify where their use in main rotor design is appropriate.

REFERENCES

1. Guffond, D.P.: Icing and De-icing Test on a 1/4 Scale Rotor in the ONERA S1MA Wind Tunnel. AIAA Paper 86-0480, Jan. 1986.

2. Reinmann, J.J.; Shaw, R.J.; and Ranaudo, R.J.: NASA's Program on Icing Research and Technology. Flight in Adverse Environmental Conditions, AGARD CP-470, 1989 (Also, NASA TM-101989).

3. Miller, T.L.; and Bond, T.H.: Icing Research Tunnel Test of a Model Helicopter Rotor. NASA TM-101978, 1989.

4. Bond, T.H.; Flemming, R.J.; and Britton, R.K.: Icing Tests of a Sub-Scale Model Main Rotor. Proceedings of the 46th Annual American Helicopter Society Forum, Vol. 1, May 1990, pp. 267-281.

5. Flemming, R.J.; Bond, T.H.; and Britton, R.K.: Results of a Sub-Scale Model Rotor Icing Test. AIAA Paper 91-0660, Jan. 1991.

6. Britton, R.K.; and Bond, T.H.: A Review of Ice Accretion Data From a Model Rotor Icing Test and Comparison Theory. AIAA Paper 91-0661, Jan. 1991.

7. Flemming, R.J.; and Lednicer, D.A.: High Speed Ice Accretion on Rotorcraft Airfoils. NASA CR-3910, 1985.

8. Scavuzzo, R.J.; and Chu, M.L.: Structural Properties of Impact Ices Accreted on Aircraft Structures. NASA CR-179580, 1987.

9. Armand, C., et al.: Techniques and Facilities Used at the ONERA Modane Centre for Icing Tests. Aircraft Icing, AGARD-AR-127, 1978, pp. A6-1 to A6-23.

10. Johnson, W.: CAMRAD/JA, A Comprehensive Analytical Model of Rotorcraft Aerodynamics and Dynamics: Johnson Aeronautics, Palo Alto, CA, 1988.

11. Keys, C.N., et al.: Estimation of Full-Scale Rotor Performance from Model Rotor Test Data. Journal of the American Helicopter Society, vol. 30, no. 4, Oct. 1985, pp. 22-29.

12. Ruff, G.A.; and Berkowitz, B.M.: Users Manual for the NASA Lewis Ice Accretion Prediction Code (LEWICE). NASA CR-185129, 1990.

13. Korkan, K.D.; Dadone, L.; and Shaw, R.J.: Performance Degradation of Helicopter Rotor Systems in Forward Flight Due to Rime Ice Accretion. AIAA 83-0029, Jan. 1983.

14. Korkan, K.D.; and Britton, R.K.: A Study of Ice Shape Prediction Methodologies and Comparison With Experimental Data. AIAA Paper 90-0753, Jan. 1990.

ORIGINAL PAGE
BLACK AND WHITE PHOTOGRAPH

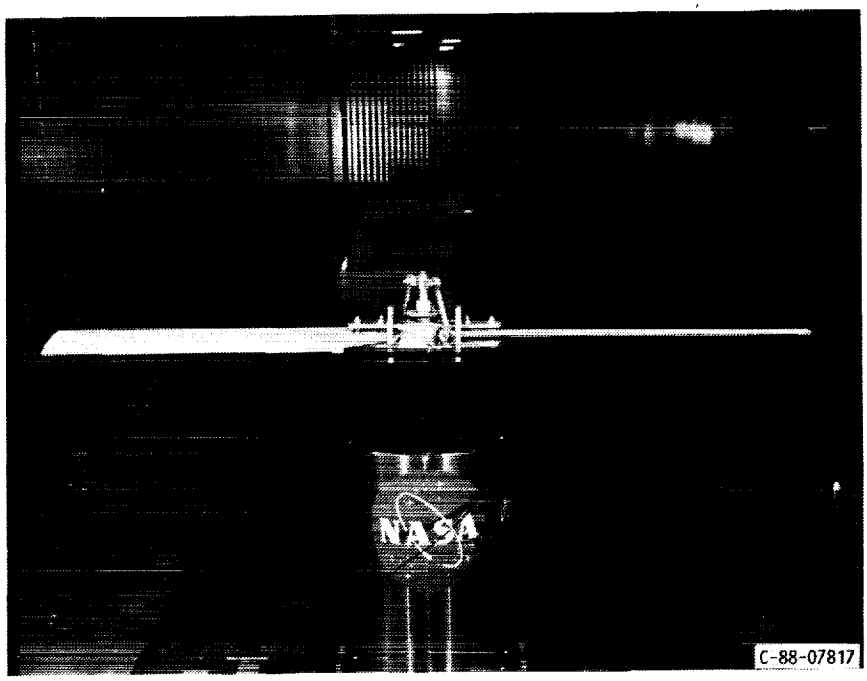

FIGURE 1. - OH-58 TAIL ROTOR ASSEMBLY.

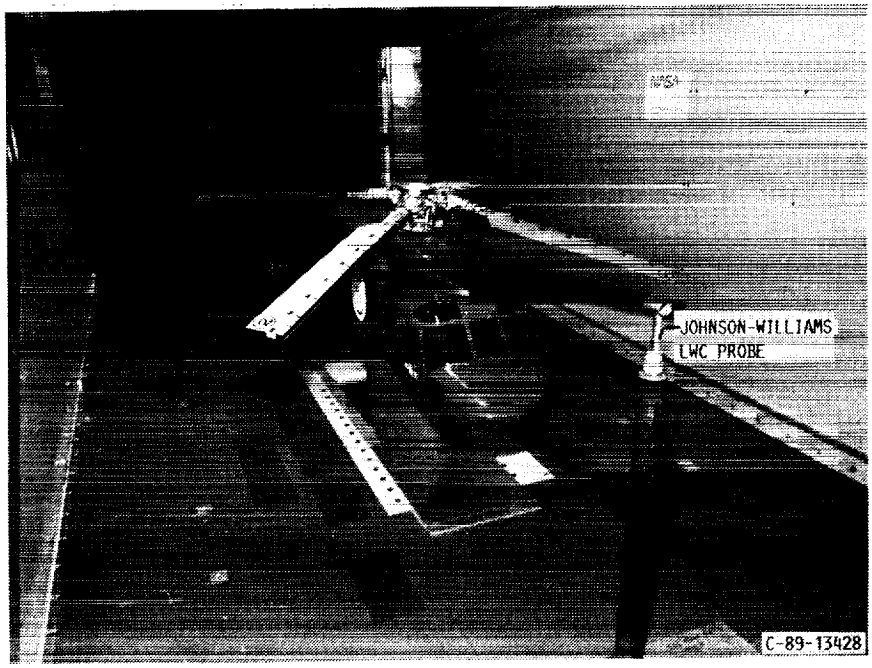

FIGURE 2. - MODEL MAIN ROTOR ASSEMBLY IN THE IRT.

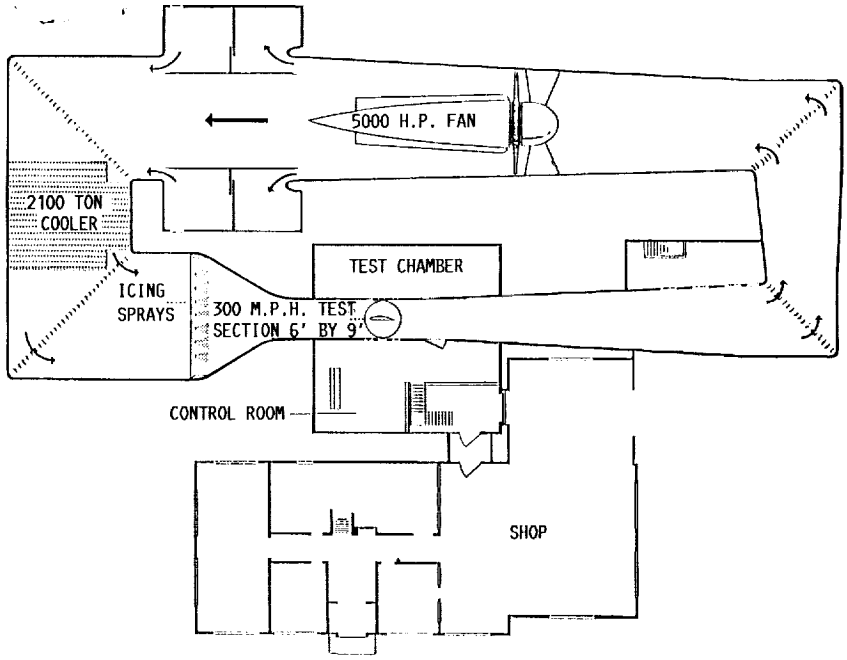

FIGURE 3. - NASA LEWIS ICING RESEARCH TUNNEL.

ORIGINAL PAGE
BLACK AND WHITE PHOTOGRAPH

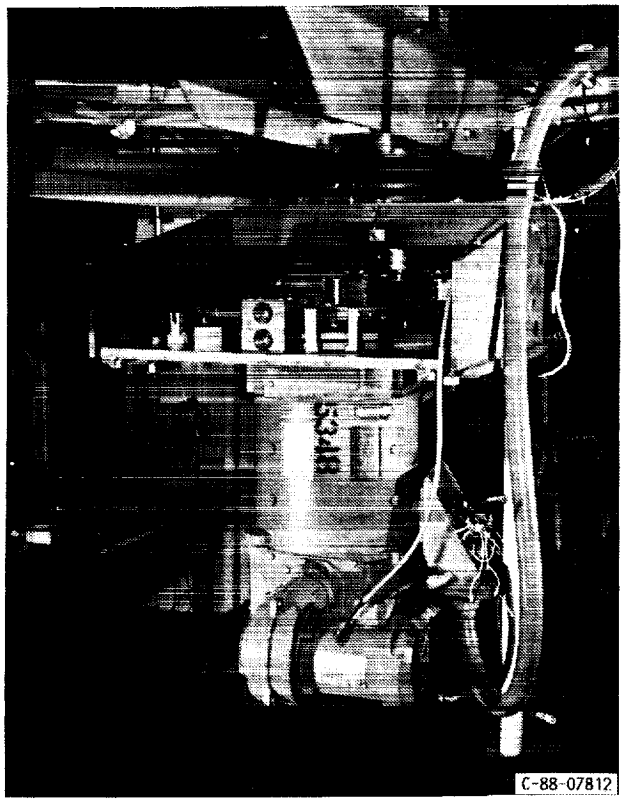

FIGURE 4. - OH-58 MODEL ROTOR DRIVE ASSEMBLY.

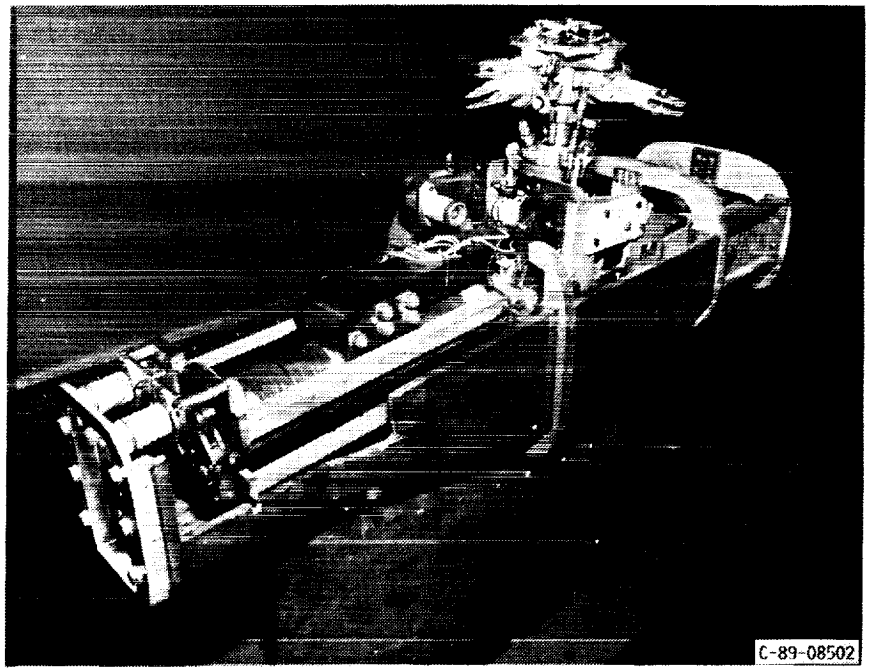

FIGURE 5. - SIKORSKY PFM ROTOR HEAD AND FORCE BALANCE ASSEMBLY.

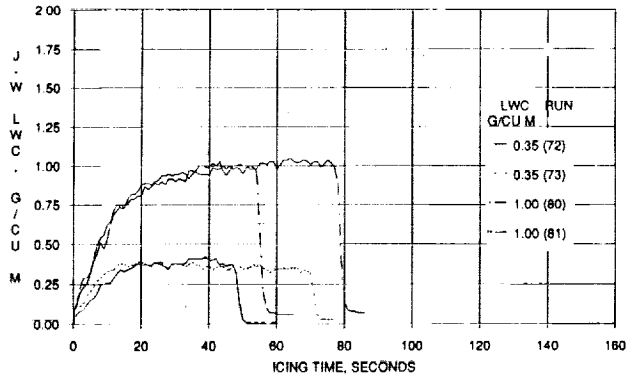

FIGURE 6. - LWC REPEATABILITY VERSUS ICING TIME (MVD = 15 μm, μ = 0.20 m/s, C_L/σ = 0.064, T = -15 ^{0}C).

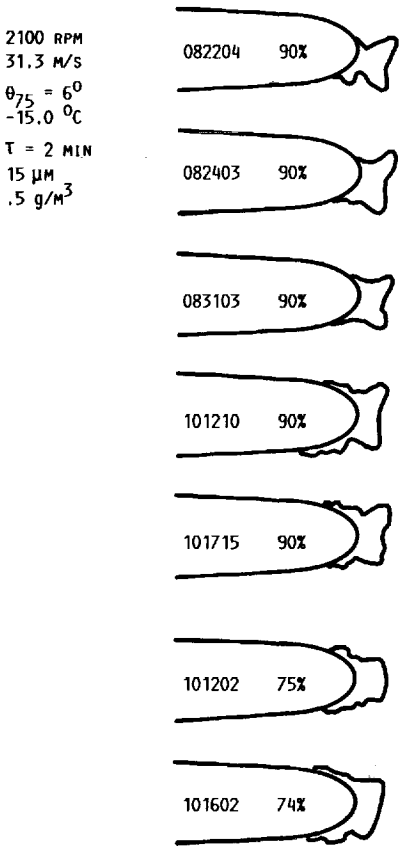

FIGURE 7. - ICE SHAPE REPEATABILITY FOR OH-58 TEST.

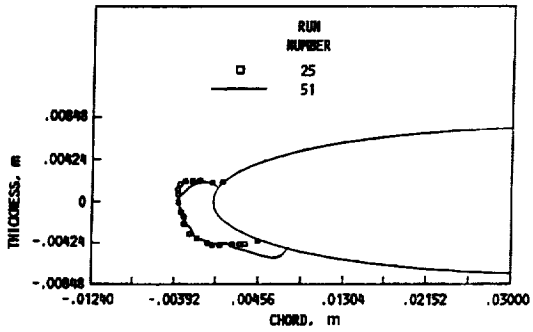

FIGURE 8. - TWO DIMENSIONAL ICE PROFILES FOR PFM TEST. (LWC = 0.5 g/m^3, MVD = 15 μm, μ = 0.20 ΩR = 183 m/s, C_L/σ = 0.064, T = -15 °C).

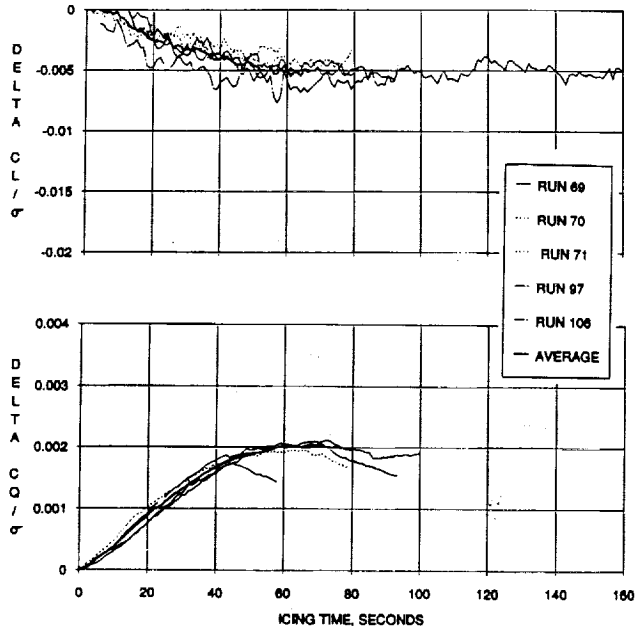

FIGURE 9. - REPEATABILITY FOR PFM TEST (ΩR = 205.7 m/s, T = -15 °C).

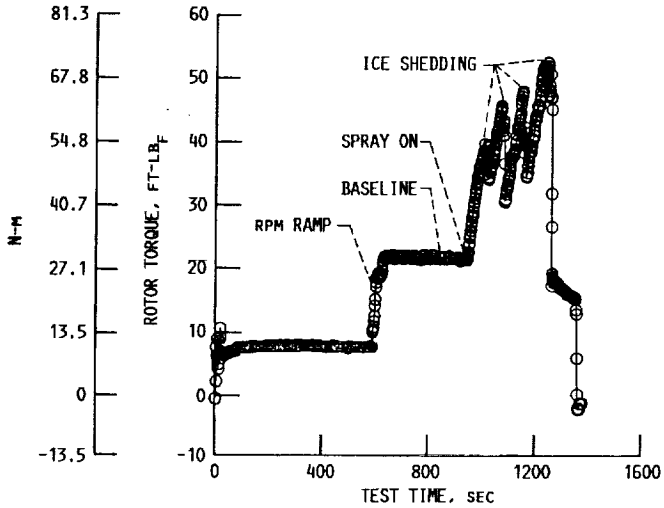

FIGURE 10. - ROTOR TORQUE VERSUS TEST TIME FOR OH-58 TEST. 2100 RPM, τ = 5.4 MIN, 15 μM, 31.3 M/S, -9.4 °C, .5 g/M^3, θ_{75} = 4° FOR OH-58.

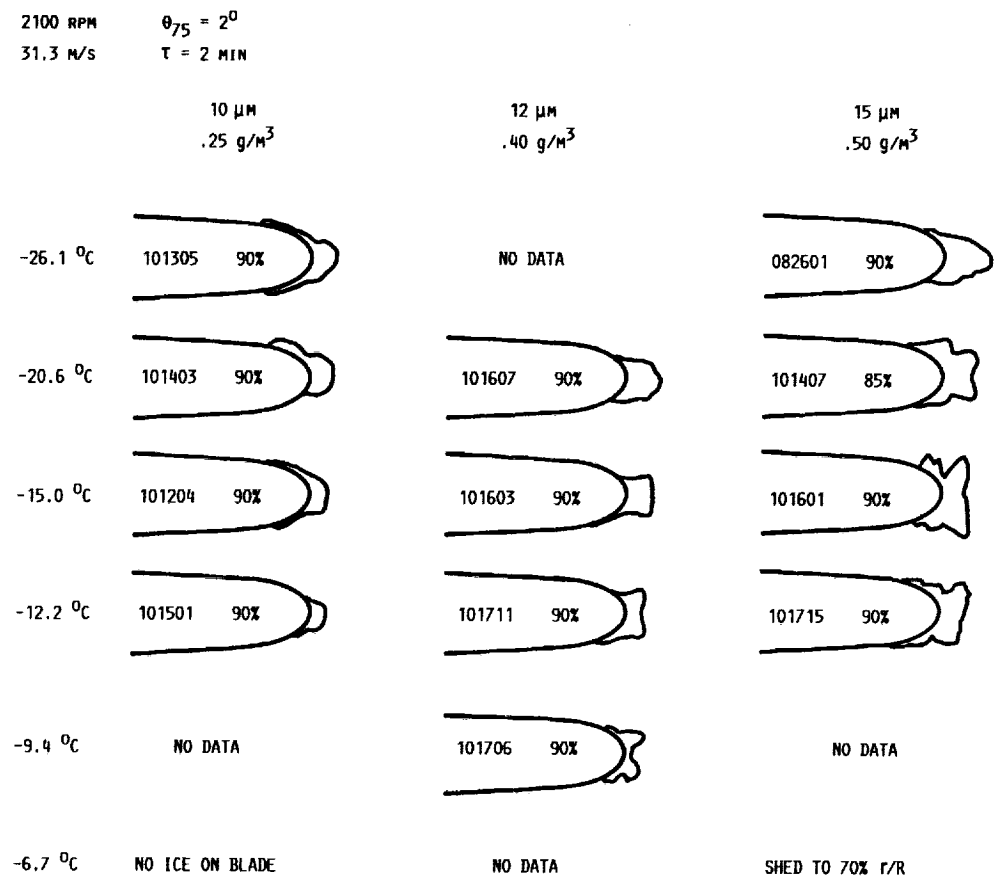

FIGURE 11. - TEMPERATURE EFFECT ON ICE ACCRETION FOR OH-58 TEST.

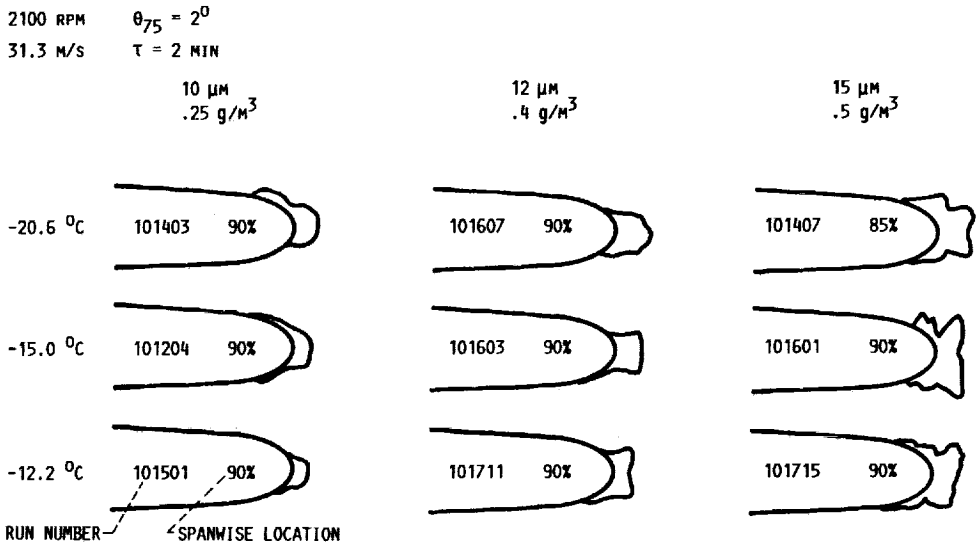

FIGURE 12(a). - LWC AND DROP SIZE EFFECT ON ICE ACCRETION FOR OH-58 TEST.

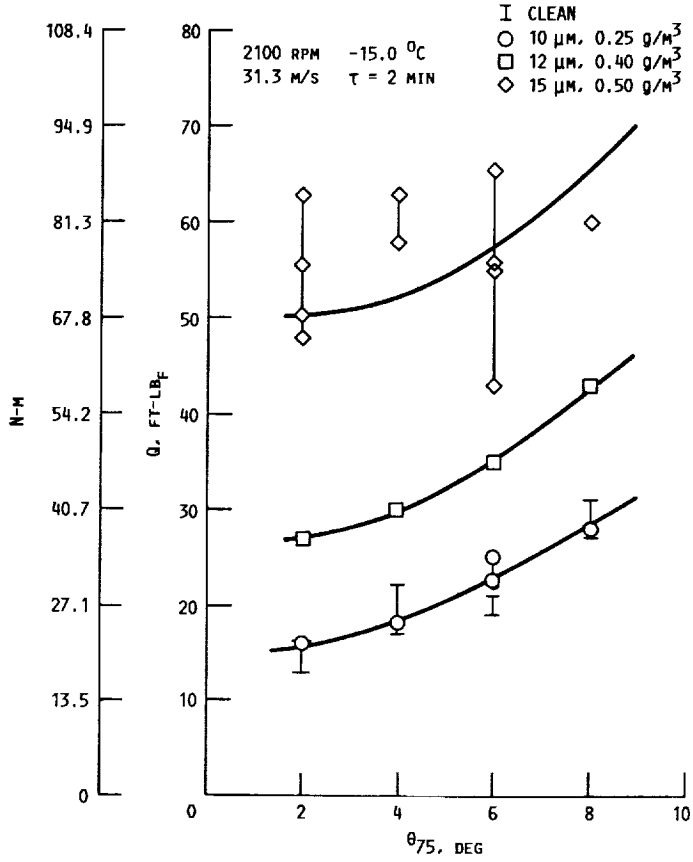

FIGURE 12(b). - LWC/DROPLET SIZE EFFECT ON TORQUE FOR OH-58 TEST.

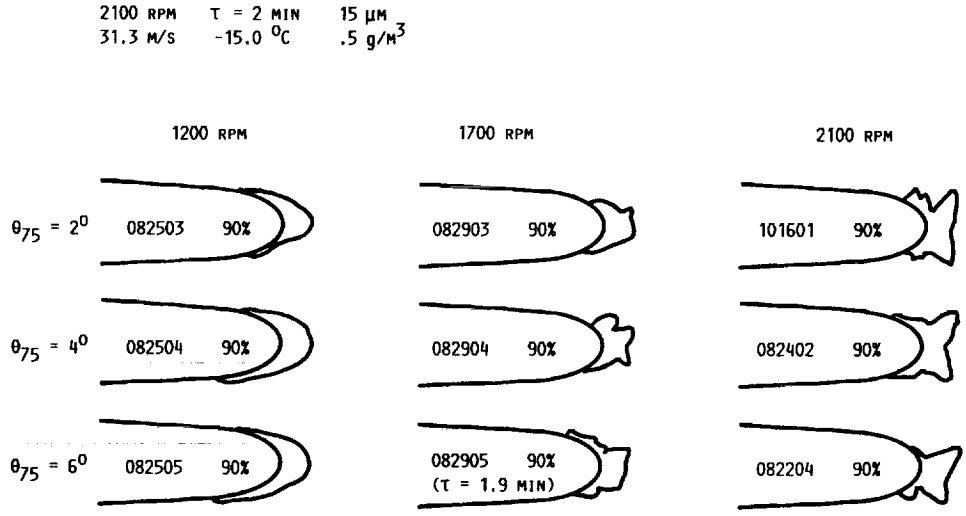

FIGURE 13. - RPM EFFECT ON ICE ACCRETION FOR OH-58 TEST.

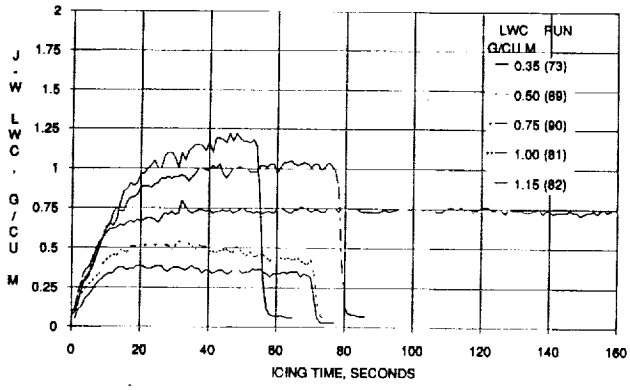

FIGURE 14. - LWC RISE TIME FOR PFM TEST (MVD = 15 μM, μ = 0.20, ΩR = 206 M/S, C_L/σ = 0.064, T = -15 ^{o}C).

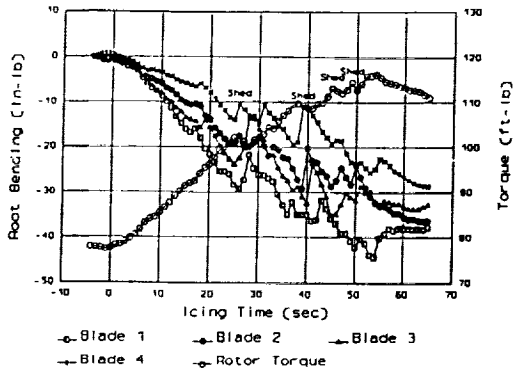

FIGURE 15. - BLADE ROOT BENDING AND TORQUE RISE VERSUS ICING TIME FOR PFM TEST. (LWC = 1.0 g/m^3, MVD = 15 μM, μ = 0.20, ΩR = 206 M/S, C_L/σ = 0.064, T = -15 ^{o}C).

ORIGINAL PAGE
BLACK AND WHITE PHOTOGRAPH

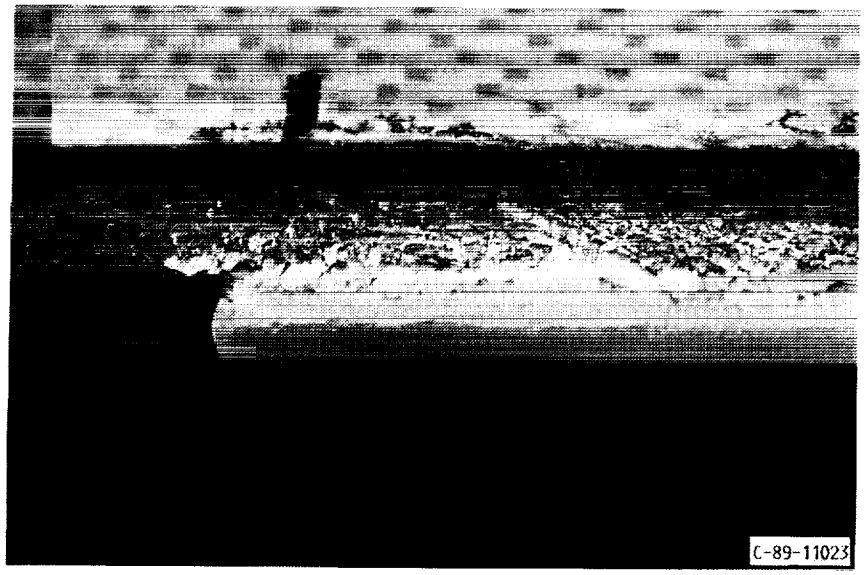

FIGURE 16. - CLOSE-UP DETAIL OF SHED ICE FROM PFM TEST.

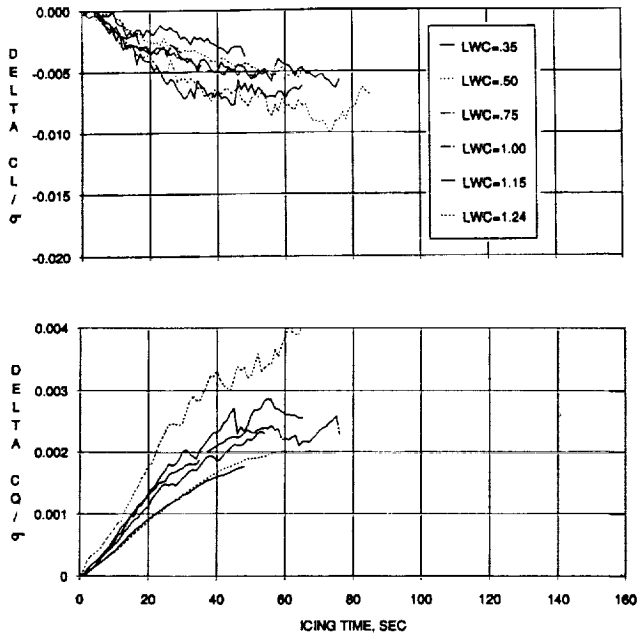

FIGURE 17. - EFFECT OF LIQUID WATER CONTENT FOR PFM TEST. ($T = -15\ ^{o}C$).

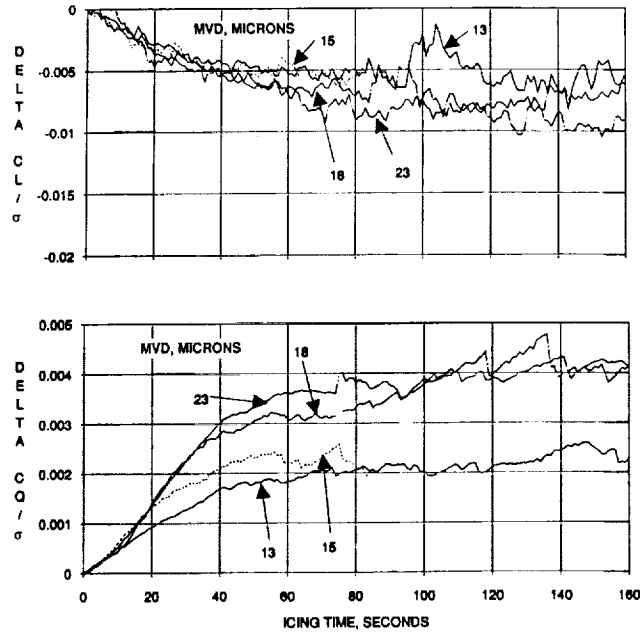

FIGURE 18. - EFFECT OF DROPLET DIAMETER FOR PFM TEST. ($LWC = 0.75\ g/m^3$).

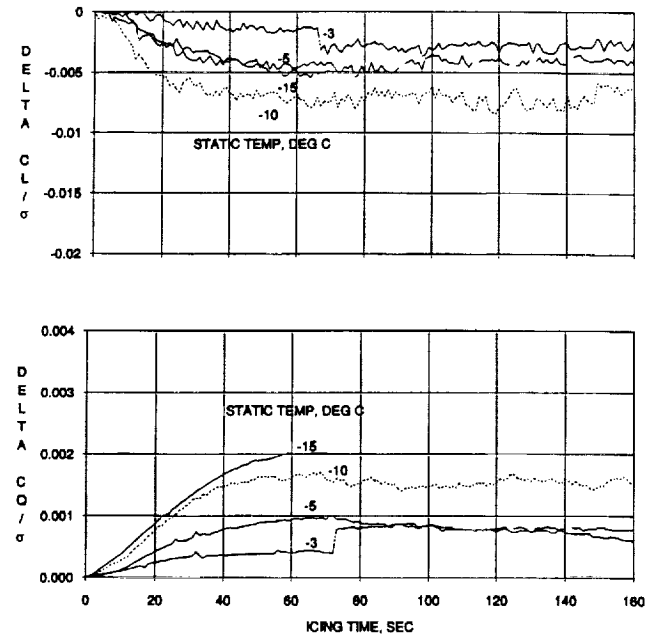

FIGURE 19. - EFFECT OF TEMPERATURE FOR PFM TEST. ($\Omega R = 205.7$ m/s, WARMER TEMPERATURE).

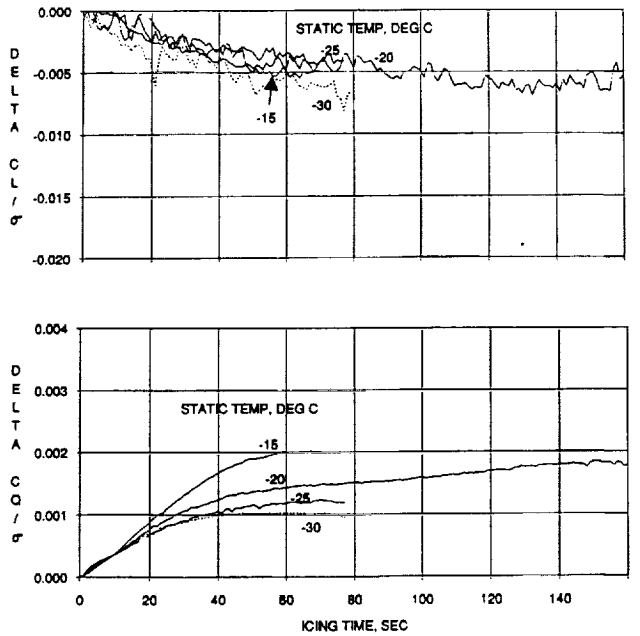

FIGURE 20. - EFFECT OF TEMPERATURE FOR PFM TEST. ($\Omega R = 205.7$ m/s, COLDER TEMPERATURE).

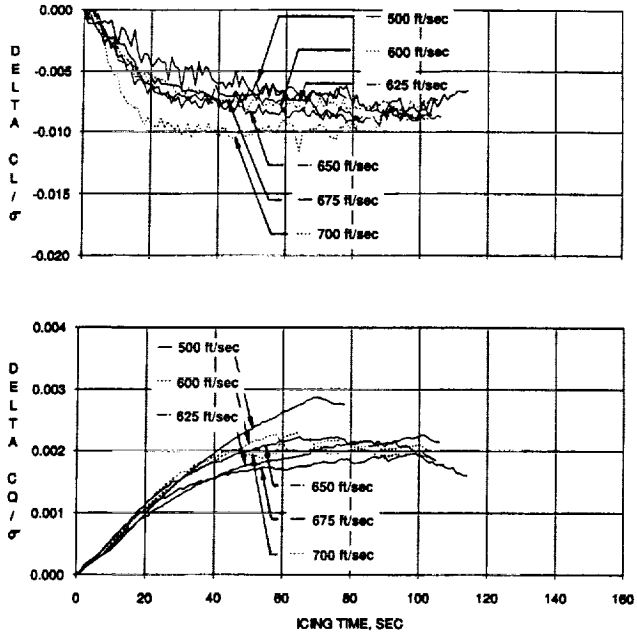

FIGURE 21. - EFFECT OF TIP SPEED FOR PFM TEST.

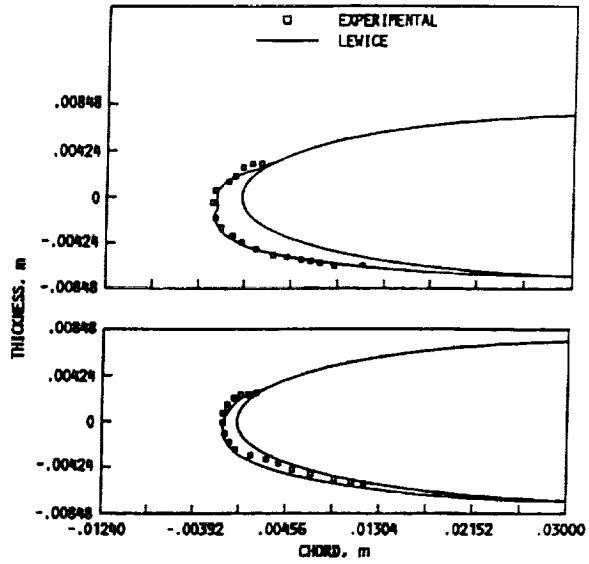

FIGURE 22. - COMPARISON BETWEEN EXPERIMENTAL AND THEORETICAL ICE SHAPES FOR PFM TEST. (LWC = 1.0 g/m^3, MVD = 15 μm, μ = 0.2, ΩR = 206 m/s, C_L/σ = 0.064, T = -15 ^{o}C).

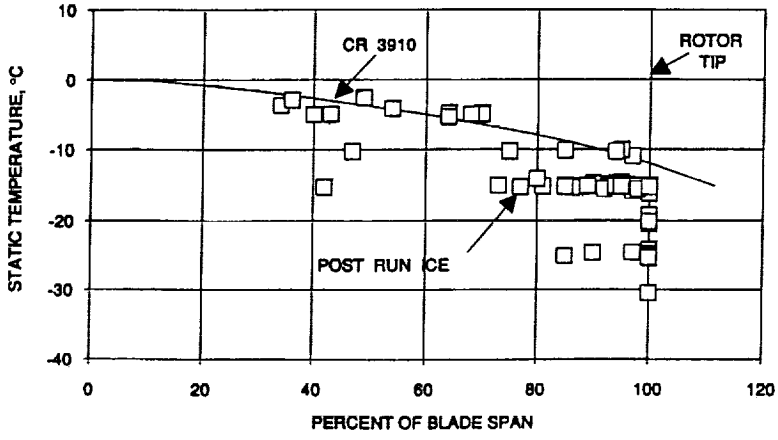

FIGURE 23. - OBSERVED AND PREDICTED MODEL ROTOR ICE EXTENT FOR PFM TEST.

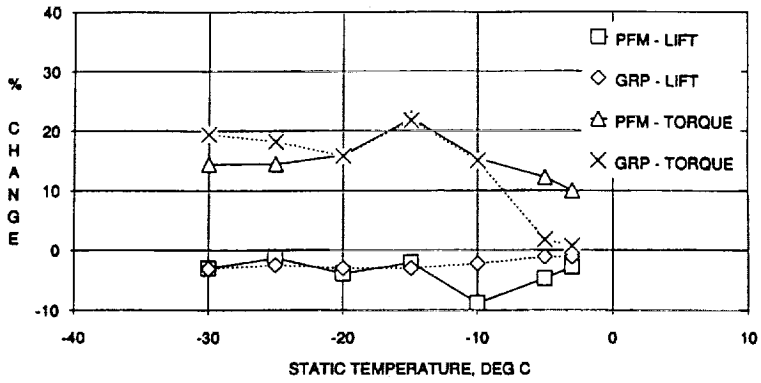

FIGURE 24. - LIFT AND TORQUE CHANGE SUMMARY FOR PFM TEST. (τ = 20 SEC, LWC = 0.5 g/M^3).

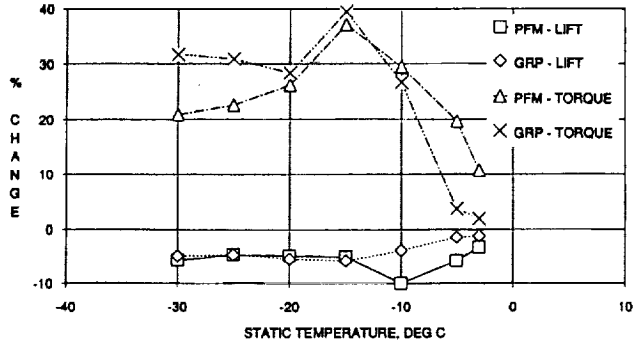

FIGURE 25. - LIFT AND TORQUE CHANGE SUMMARY FOR PFM TEST. (τ = 40 SEC, LWC = 0.5 g/M^3).

NASA
National Aeronautics and Space Administration

Report Documentation Page

1. Report No.	2. Government Accession No.	3. Recipient's Catalog No.
NASA TM -104351		

4. Title and Subtitle	5. Report Date
Model Rotor Icing Tests in the NASA Lewis Icing Research Tunnel	
	6. Performing Organization Code

7. Author(s)	8. Performing Organization Report No.
Robert J. Flemming, Randall K. Britton, and Thomas H. Bond	E - 6136
	10. Work Unit No. 505 - 68 - 11

9. Performing Organization Name and Address	11. Contract or Grant No.
National Aeronautics and Space Administration Lewis Research Center Cleveland, Ohio 44135 - 3191	
	13. Type of Report and Period Covered Technical Memorandum

12. Sponsoring Agency Name and Address	14. Sponsoring Agency Code
National Aeronautics and Space Administration Washington, D.C. 20546 - 0001	

15. Supplementary Notes

Prepared for the 68th Meeting of the Fluid Dynamic Panel Specialists Meeting on Effects of Adverse Weather on Aerodynamics sponsored by the Advisory Group for Aerospace Research and Development, Toulouse, France, April 29-May 1, 1991. Robert J. Flemming, United Technologies Corporation, Sikorsky Aircraft Division, 6900 Main Street, Stratford, Connecticut 06601; Randall K. Britton, Sverdrup Technology, Inc., Lewis Research Center Group, 2001 Aerospace Parkway, Brook Park, Ohio 44142; Thomas H. Bond, NASA Lewis Research Center.

16. Abstract

Tests of a lightly instrumented two-bladed teetering rotor and a heavily instrumented sub-scale articulated main rotor were conducted in the NASA Lewis Research Center Icing Research Tunnel (IRT) in August 1988 and in September and November 1989, respectively. The first was an OH-58 tail rotor which had a diameter of 1.575 m (5.17 ft) and a blade chord of 0.133 m (5.25 in), and was mounted on a NASA designed test rig. The second, a four bladed articulated rotor, had a diameter of 1.83 m (6.00 ft) and the 0.124 m (4.9 in) chord blades were specially fabricated for the experiment. This rotor was mounted on a Sikorsky Aircraft Powered Force Model, which enclosed a rotor balance and other measurement systems. The models were exposed to variations in temperature, liquid water content, and median droplet diameter, and were operated over ranges of advance ratio, shaft angle, tip Mach number (rotor speed), and weight coefficient to determine the effect of these parameters on ice accretion. In addition to strain gage and balance data, the test was documented with still, video, and high speed photography, ice profile tracings, and ice molds. This paper presents the sensitivity of the model rotors to the test parameters, and compares the results to theoretical predictions.

17. Key Words (Suggested by Author(s))	18. Distribution Statement
Icing Rotorcraft Wind tunnel test	Unclassified - Unlimited Subject Category 07

19. Security Classif. (of the report)	20. Security Classif. (of this page)	21. No. of pages	22. Price*
Unclassified	Unclassified	26	A03

NASA FORM 1626 OCT 86

*For sale by the National Technical Information Service, Springfield, Virginia 22161